Sensors & Transducers Journal, Vol. 137, Issue 2, February 2012, pp. 123-136

www.sensorsportal.com

Sensors & Transducers

ISSN 1726-5479

http://www.sensorsportal.com

Preparation and Study of H_2S Gas Sensing Behavior of $ZnFe_2O_4$ Thick Film Resistors

*** S. V. BANGALE, S. R. BAMANE**

Metal Oxide Research, Laboratory, Department of Chemistry, Dr. Patangrao Kadam Mahavidyalaya, Sangli 416416 (M.S.) India

Tel.: 0233-2535993, fax: 0233-2535993

E-mail: bangale_sv@rediffmail.com

Received: 5 January 2012 /Accepted: 14 February 2012 /Published: 28 February 2012

Abstract: Semiconductive nano-sized $ZnFe_2O_4$ material is synthesized by a solution combustion method using inorganic reagents as $Zn(NO_3)_3$. $6H_2O$, $Fe(NO_3)_3.6H_2O$, and glycine as a fuel. This process is a convenient, environment friendly, inexpensive and efficient for the preparation of $ZnFe_2O_4$ nanomaterial. The synthesized material is characterized by Thermo gravimetric Differential analysis (TG/DTA), X-ray Diffraction studied (XRD), Energy dispersive X-ray microanalysis studies (EDX), Scanning Electron Microscopy (SEM) and Transmission Electron Microscopy (TEM) techniques. Conductance response of the nanocrystalline $ZnFe_2O_4$ thick film is measured by exposing the film to reducing gases like hydrogen sulphide (H_2S), ammonia (NH_3), acetone, carbon dioxide (CO_2), hydrogen (H_2), and ethanol. The sensor exhibited a fast response and a good recovery. The results demonstrated that $ZnFe_2O_4$ can be used as a gas-sensing material which has a high sensitivity and good selectivity to hydrogen sulphide (H_2S) at 1000 ppm.

Keyword: Combustion reaction, TEM, Thick film, $ZnFe_2O_4$ nanoparticles, Gas sensor.

1. Introduction

The need for a novel gas sensor material capable of providing reliable operation in harsh environments is now greater than ever. Such sensors find a range of applications, including the monitoring of traffic pollutants or food quality in specially designed electronic noses [1, 2]. Semiconductor metal oxide sensors are alternatives for non expensive and robust detection system. Spinel-type oxide semiconductors with formula MFe_2O_4 have been reported to be sensitive materials to both oxidizing and reducing gases [3]. Liu et al [4] reported the high sensitivity of $CdFe_2O_4$ to ethanol vapour; Reddy

et al [5] investigated $NiFe_2O_4$ as sensor to detect Cl_2 in air. A few Cl_2 gas sensors have already been developed, Transparent conducting oxide (TCO) thin film sensors operate at higher temperature (~300^0C). However it is inconvenient to operate. It is therefore, essential to develop a sensor, which could detect Cl_2 gas at room temperature. Zirconia tubes, $MgO\text{-}In_2O_3$, $Zn_2O_5\text{-}MgIn_2O_4$ (TCO), ZnO-CaO etc., are materials utilized in Cl_2 sensing applications [6-10]. Chen et al [11] revealed that $MgFe_2O_4$ and $CdFe_2O_4$ are sensitive and selective to LPG and C_2H_2. Other earlier report about the application study of zinc ferrite as a gas sensing material include $ZnFe_2O_4$ particles to H_2S [12], a directly deposited film to Co [13], ultrafine powder to Cl_2[14]CdO-doped $ZnFe_2O_4$ to ethanol[15], a $ZnO/ZnFe_2O_4$ thick film to propanol [16], $ZnFe_2O_4$ tubes synthesis and application to gas sensors [17]. Our latest work about MCo_2O_4 (M = Ni, Cu, Zn) nanotubes, which possess combined characteristics of hallow-inside and 1D structure, has displayed excellent selectivity and high sensitivity [18]. In these regards, zinc ferrite tubes, which not only hold the above mentioned 1D tubular structure but also have advantages of low cost and environmental friendliness, are expected to be a good candidate as sensor materials.

The most general adsorption-desorption gas sensing mechanism of semiconductors gas sensors is the simple resistivity change, due to the desorption of surface oxygen adsorbates via reactions with reducing gases such as H_2S, CO, and H_2. The p-n heterocontact a concept is used in the present investigation, instead of adsorption-desorption mechanism, which was introduced in 1979 and has been applied as humidity sensors, liquid sensors and gas sensors. The heterocontact concept was found to be very effective for the H_2S gas sensing at room temperature. Room temperature gas detection offers advantages of low power drain and reduced tendency to provide a source of ignition. The hetrocontact type sensors have an intrinsic difference in behavior from those based on catalytic oxidation/reduction of gas molecules [19]. The heterocontact type work on the principle of a barrier mechanism, which need no adsorption and desorption of oxygen for the detection of H_2S gas. Some well-known materials for H_2S gas sensing are SnO_2-CuO [20], $CuO\text{-}SnO_2$-ZnO [21], SnO_2-Pd [22], $SnO_2\text{-}Al_2O_3$ [23], SnO_2-CuO-SnO [24] and $ZnSb_2O_6$ [25].

Herein, we prepared $ZnFe_2O_4$ nanopowder by this simple solution combustion reaction. One of our aims is to develop a general synthesis method and explore the gas sensing properties of the $ZnFe_2O_4$ nanopowder obtained. We found that the process is a convenient, environment friendly, inexpensive and efficient for preparation of $ZnFe_2O_4$ nanomaterial with the grain size of about 15-35 nm. Furthermore, the $ZnFe_2O_4$ obtained possesses excellent gas-sensing responses to reducing gas. In the present paper we report the development of thick film zinc iron oxide H_2S sensors.

2. Materials and Methods

2.1. Materials

All the reagents are of analytical grade and are used as received without further purification. Zinc nitrate [$Zn(NO_3)_26H_2O$], ferric nitrate [$Fe(NO_3)_26H_2O$], glycine are purchased from Sigma-Aldrich chemical reagents Co. (USA).

2.2. Methods

In this study, $ZnFe_2O_4$ powder was synthesized by solution combustion technique using the starting regents as $Zn(NO_3)_26H_2O$ (7.43 g), Fe $(NO_3)_26H_2O$ (7.27 g) and glycine (6.05 g) as a fuel. Glycine possesses a high heat of combustion. It is an organic fuel providing a platform for redox reactions during the course of combustion. Initially the zinc nitrates, iron nitrates and glycine are taken in the 1:1:4 stoichiometric amount and homogenous paste was made. The paste formed was evaporated on

hot plate in temperature range of 70 to 80 ^{0}C to result into a thick gel. The gel was kept on a hot plate for auto combustion and heated in the temperature range of 170 to 180 ^{0}C. The nanocrystalline $ZnFe_2O_4$ powder was formed within five minutes. The powder was sintered at 300, 500, 800, and 1000 ^{0}C for 4 hr. which resulted in to a brown color shining powder [26-27].

2.3. Thick Film Preparation

Zinc iron oxide powder was ground in an agate pastel-moter to ensure sufficiently fine particle size. The fine powder was calcined at 800 ^{0}C for 12 h in air and re-ground. The thixotropic paste [28-29] was formulated by mixing the resulting $ZnFe_2O_4$ fine powder with a solution of ethyl cellulose (a temporary binder) in a mixture of organic solvents such as butyl carbitol acetate and turpineol. The ratio of inorganic and organic path was kept as 75:25 in formulating the paste. The paste was then used to prepare thick films. The thixotropic paste was screen printed on a glass substrate in desired patterns. The films prepared were fired at 500 ^{0}C for 24 h.

2.4. Characterization Technique

The project describes a simple and cost-effective way of preparing of $ZnFe_2O_4$ nanoparticles by auto combustion method using zinc and ferric nitrates, glycine as fuel. Further it illustrates the structural, chemical composition, thermal morphology and gas sensing study of the samples using Thermo gravimetric Differential analysis (TG/DTA), X-ray diffraction (XRD), particle size analyzer high-resolution scanning electron microscopy (HR-TEM), transmission electron microscopy (TEM), and static gas sensing units to studied sensing properties.

2.5. Fabrication and Analysis of Gas Sensors

The sensing performance of the sensors was examined using a “static gas-sensing system. There were electrical feeds through the base plate. The heat was fixed on the base plate to heat the sample under test up to the required operating temperatures. The current passing through the heating element was monitored using a relay with adjustable ON and OFF time intervals. A Cr-Al thermocouple was used to sense the operating temperature of the sensors. The output of the thermocouple was connected to digital temperature indicators. A gas inlet valve was fitted at one port of the base plate. The required gas concentration inside the static system was achieved by injecting a known volume of test gas using a gas-injecting syringe. A constant voltage was applied to the sensors, and current was measured by a digital Pico-ammeter. Air was allowed to pass into the glass dome after every Gases exposure cycle.

3. Result and Discussion

3.1 Spinel Structure and Formation Analysis

TG-DTA analysis was performed at a heating rate of 10 K min^{-1} to investigate the thermal properties of $ZnFe_2O_4$. The TG spectrum and its 1st derivative in Fig. 1 show the thermal decomposition of $ZnFe_2O_4$ is the curve indicates that the slight weight loss in $ZnFe_2O_4$ powder due to little loss about 14.66 at temperature up to 200 ^{0}C in $ZnFe_2O_4$ of moisture, carbon dioxide and nitrogen gas. The DTA curve of $ZnFe_2O_4$ recorded in static air and in shown in Fig. 1. The curve shown that $ZnFe_2O_4$ did not decompose, but weight loss was due to dehydrogenation, decarboxylation and denitration. Further weight loss of about 16 % between the temperature range 400 ^{0}C and continuous loss in weight about 33.33 % up to 550 ^{0}C is attributed to loss of organic materials and yield final product at 600 ^{0}C.This

weight loss and weight gained was very negligible. This weight change was in the range of 800 ^{0}C these indicating that the synthesized powder was almost stable from the beginning. The formation temperature in the present work is found to be comparatively similar than that reported for corresponding solid state reaction route as shown in reaction.

$$2C_2NH_3O_2 + (9/2)\ O_2 \rightarrow N_2 \uparrow + 4CO_2\uparrow + 5H_2O$$

$$Zn\ (NO_3)_3 + Fe\ (NO_3)_3 + 4C_2H_5NO_2 \rightarrow ZnFe_2O_4 + 8H_2O + 10H_2O + 5N_2 \uparrow$$

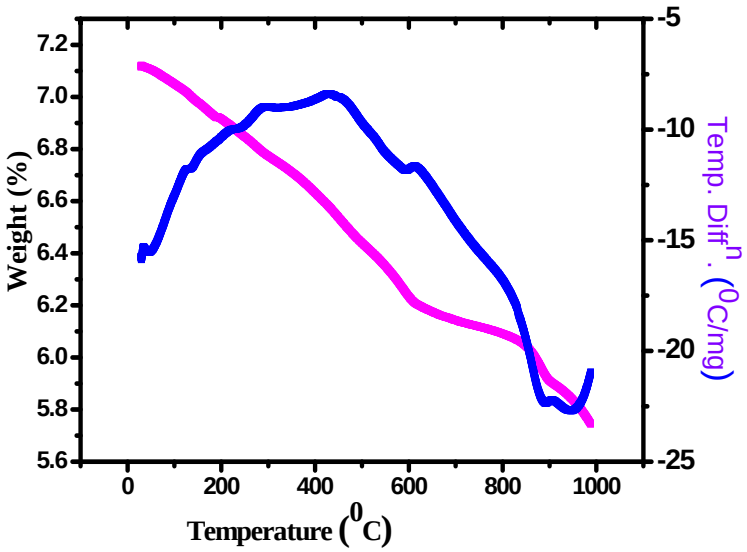

Fig. 1. Thermo gravimetric Differential analysis TG-DTA curve of mixed precursor $ZnFe_2O_4$.

3.2. X-Ray Diffraction Analysis

The X-ray diffraction pattern of $ZnFe_2O_4$ powder is shown in Fig. 2 The observed d values compared with standard d values and are in good agreement with standard d value JCPDS data card number 82-1042. The structure possesses the cubic may be attributed to the different preparation method which may yield different structural defects. The crystalline size was determined from full width of half maximum (FWHM) of the most intense peak obtained by shown scanning of X-ray diffraction pattern. The grain size was calculated by using Scherrer's formula [30-31].

$$d = 0.9\lambda/\ \beta\cos\theta,$$

where, d is the crystalline size, λ is the X-ray wavelength of the Cu K_α source (λ=1.54056 A^0), β is the FWHM of the most predominant peak at 100 % intensity, θ is the Braggs angle at which peak is recorded. In order to obtain pure nanocrystalline $ZnFe_2O_4$ particles and understand the thermal characterizations, the as prepared $ZnFe_2O_4$ powder is further calcined at 180, 300, 500, 800 and 1000 ^{0}C respectively (the calcined temperature assigned as T_C). Fig. 2 present XRD patterns for $ZnFe_2O_4$ oxide nanoparticles. The effects of the calcinations temperature on the crystallite size of $ZnFe_2O_4$ particles can be demonstrated. Traces of $ZnFe_2O_4$ crystallites phases (111), (311), (400), (422) and (511) are detected in the XRD pattern for all calcined temperatures and then their intensities increase abruptly when the T_C above 1000 ^{0}C .In general, the sharpness of the XRD peak (i.e. high crystallinity) is increased as the T_C increases. According to the (311) diffraction pattern of $ZnFe_2O_4$ crystalline, the particle size of $ZnFe_2O_4$ can be calculated from the full width at haif-maximum using the Scherrer equation. Obviously, the particle size of $ZnFe_2O_4$ changes as the *Tc* controlled fewer than

180, 300, 500, 800 and 1000^{0}C, the order is 22, 23, 25, 32 and 33 nm, respectively. These indicate that the crystallinity of $ZnFe_2O_4$ is accelerated as the *Tc* above 500 ^{0}C. It illustrates the relationship between the annealing temperature and the average crystal size of the $ZnFe_2O_4$ nanoparticles. It is obvious that the $ZnFe_2O_4$ nanoparticle grows slowly at 300-500 ^{0}C and 800-1000 ^{0}C, respectively, the nanoparticle grow rapidly at 800 ^{0}C.

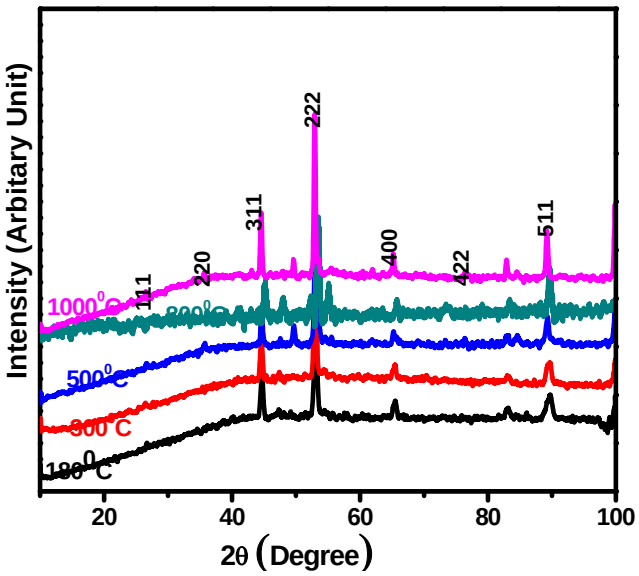

Fig. 2. XRD pattern of calcinied mixed precursor $ZnFe_2O_4$ at 180 ^{0}C, 500 ^{0}C, 800 ^{0}C, 1000 ^{0}C, in air for 4 h.

3.3. Particle Size Analysis

Particle size distribution studies have been carried out by using dynamic light scattering Fig. 3 techniques (DLS) Via Laser input energy of 632 nm). It was observed that Zinc iron oxide nanoparticles have narrow size distribution within the range of about 25-30 nm. Fig. 4 which well matches with calculated from Debye-Scherrer equation.

3.4. EDX Analysis

The elemental analysis of the sample was carried out by using energy dispersive X-ray spectrometer (EDS) and is shown in Fig. 4. The EDS result clearly shows that $ZnFe_2O_4$ contains Zn, Fe, and O without any impurity. Quantitative EDX analysis verified that doping with Zinc is close to the expected concentration.

3.4. SEM Analysis

The microstructure of the sintered samples can be visualized from scanning electron microscope (SEM) tool. Fig. 5 shown the particle morphology of low and high a resolution, the particles are most irregular in shape with a Nanosize range. Some particles are found as agglomerations containing very fine particles the particles shapes are not defined porous nature and small and large core approximately spongy pores are seen in the micrograph.

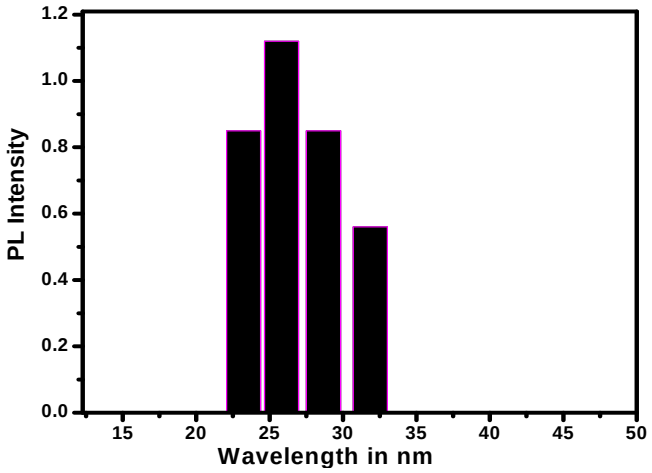

Fig. 3. Particle size distribution studies.

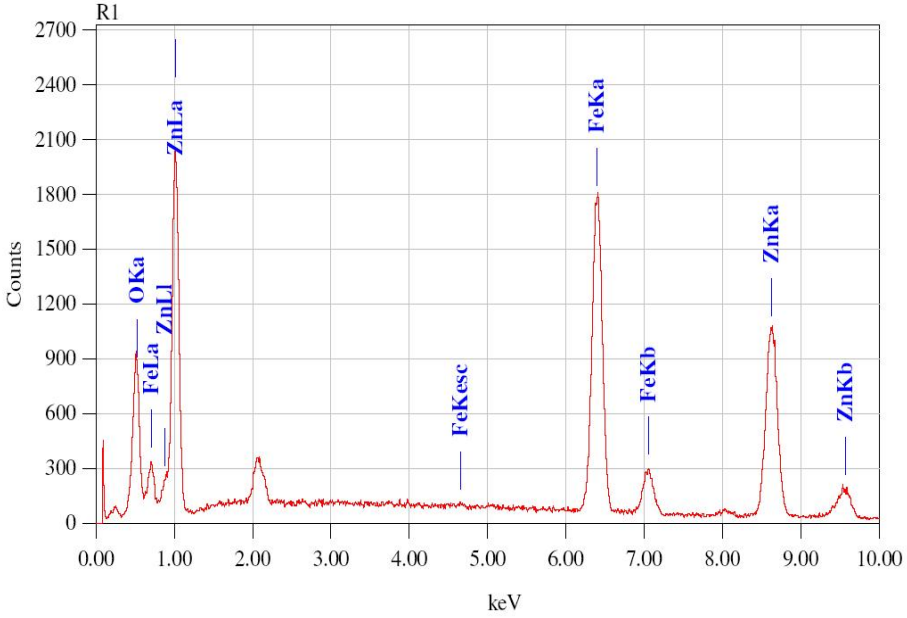

Fig. 4. EDX pattern of mixed precursor at 800 ^{0}C in air for 4 h.

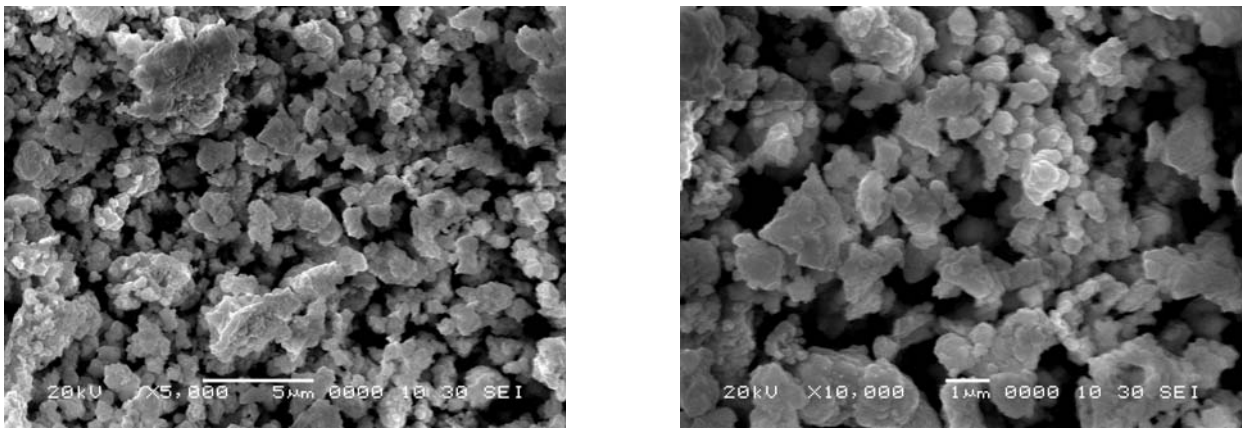

(a) (b)

Fig. 5. SEM images of mixed precursor at 800 ^{0}C in air for 4 h (a) low resolution, and (b) high resolution.

3.5. TEM Analysis

The TEM specimens were prepared by placing micro drops of colloid solutions on a carbon film supported by a copper grid. The TEM image of the mixed precursor calcined at 800 ^{0}C in air for 4 h are shown in Fig. 6 (a, b, c). It indicates the presence of $ZnFe_2O_4$ nanoparticles with size 30-40 nm which form spherical type of oriental aggregation throughout the region, which are correlated well with the XRD result. The selected area electron diffraction (SAED) pattern Fig. 6 (d) shows the spot type pattern which is indicative of the presence of single crystalline particles. No evidence was found for more than one pattern, suggesting the single phage nature of the material.

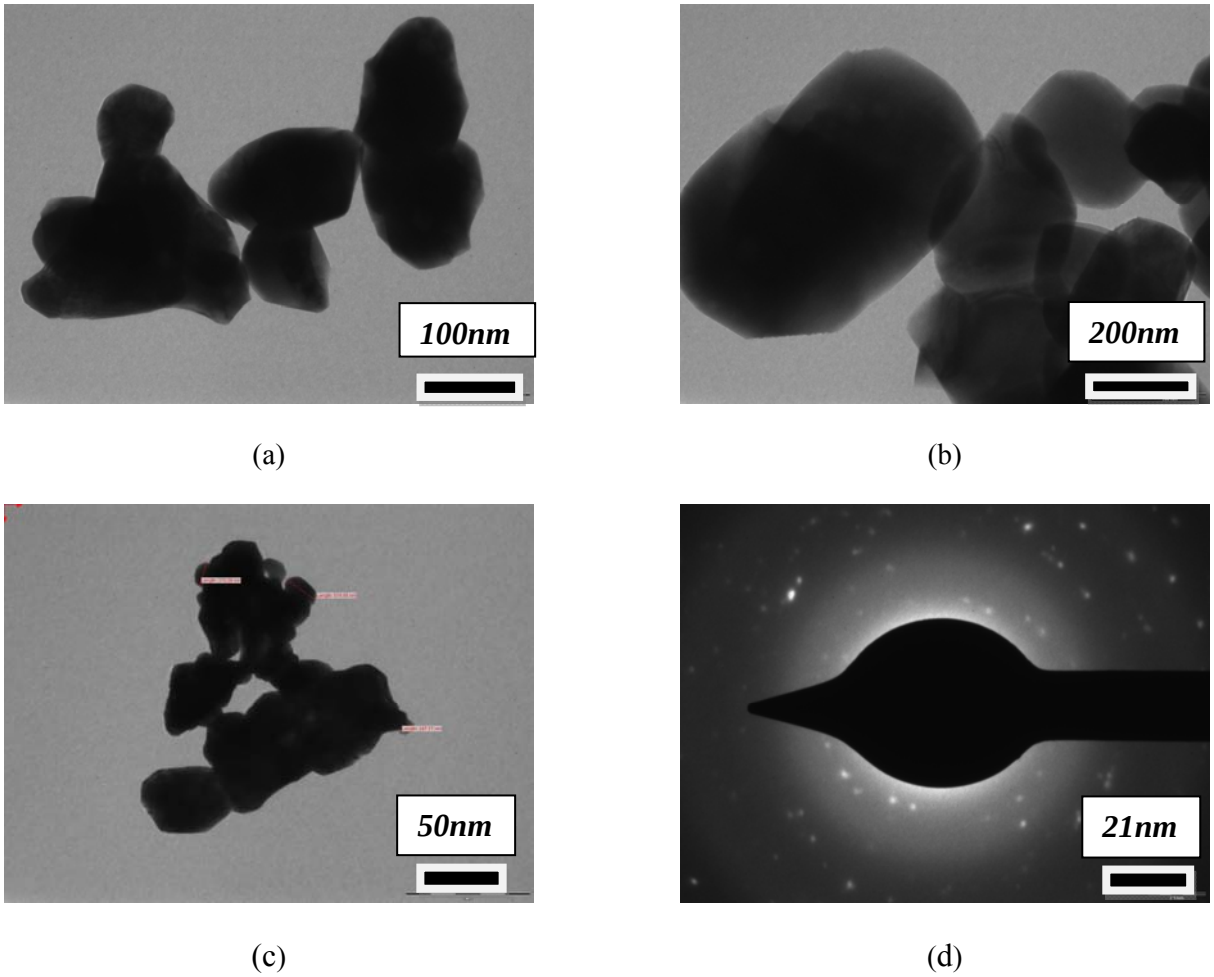

(a) (b)

(c) (d)

Fig. 6. TEM images with corresponding SAED patterns of the $ZnFe_2O_4$ samples calcined in air for 4 h at (a, b, c, d) 800 ^{0}C.

4. Electrical Properties

4.1. I-V Characteristics

Fig. 7 depicts I-V characteristics of $ZnFe_2O_4$ films. It is clear from the symmetrical I-V characteristics that the silver contacts on the films were ohmic in nature.

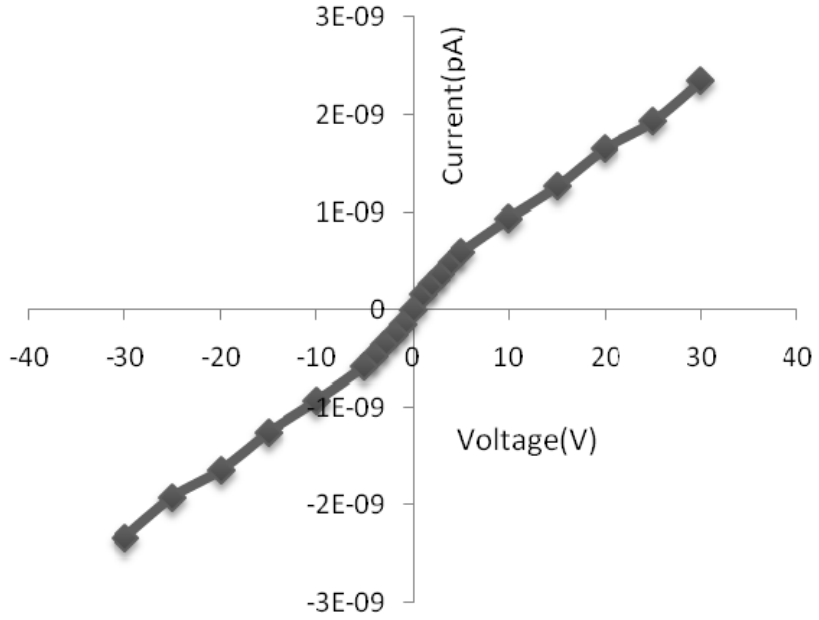

Fig. 7. *I-V* characteristics of the sensor.

4.2. The Conductance of $ZnFe_2O_4$ Sensors

Fig. 8 shows the conductance-temperature behavior of $ZnFe_2O_4$ based sensors in air a conductance peak occurring in the C-T curve at about 400 ^{0}C indicates the characteristic of atypical surface-controlled sensor model [32]. In air, from 30 to 400 ^{0}C, the conductance of sensor increases with the increasing of temperature, that is the intrinsic characteristic of semiconductor, but the oxygen chemically adsorbed on the surface of $ZnFe_2O_4$ undergoes the following reactions with the temperature increasing,

$$O_{2(ad)} \leftrightarrow O^-_{2(ad)} \leftrightarrow 2O^-_{(ad)} \leftrightarrow 2O^{2-}_{(ad)}$$

When temperature increases, the equilibrium moves to the right, $O_{2(ad)}$ captures the electrons from the conduction band of sensor, result in the decrease of conductance. When temperature is higher than 400 ^{0}C, the effect of equilibrium (3) on the conductance play a major role that leads to the conductance decreasing of sensor. The gas sensing mechanism is based on the changes of the surface conductance of $ZnFe_2O_4$. The reducing gas R acting on the surface of $ZnFe_2O_4$ can be described as:

$$2e^- + O_2 \rightarrow 2O^-$$

$$O^- + R \rightarrow RO\ e^- ,$$

where e- represents a conduction band electron, In the absence of reducing gas R, electron are removed from the $ZnFe_2O_4$ conduction band by the reduction of O_2, resulting in the formation of O^- species and consequently the conductance of $ZnFe_2O_4$ decrease. When R is introduced, it react with surface-absorbed oxygen species O^- to from RO, and electron enter into the conduction band of $ZnFe_2O_4$, leading to increase in conductance.

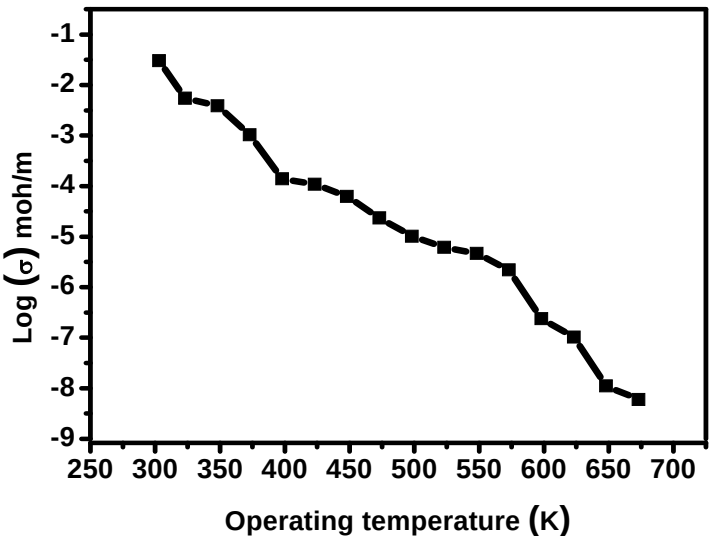

Fig. 8. Variation of Resistivity with reciprocal operating temperature.

5. Sensing Performance of the Sensor

5.1. Measurement of Gas Response, Selectivity, Response and Recovery Time

Gas response (S) is defined as the ratio of the change in conductance of the sensor on exposure to the target gas to the original conductance in air. The relation for S is as: $S = G_g - G_a / G_a$,where G_a and G_g are the conductance of sensor in air and in a target gas medium, respectively.

Selectivity or specificity is defined as the ability of a sensor to respond to a certain gas in the presence of other gases. The time taken for the sensors to attain 90 % of the original conductance is the recovery time.

5.2. Sensing Performance of $ZnFe_2O_4$ Thick Films

5.2.1. Gas Response and Operating Temperature

Fig. 9 depicts the variation of 1000 ppm gas responses with operating temperature. The $ZnFe_2O_4$ sensor was observed to be a temperature dependent gas sensor. From Fig. 9 it is observed that the sensor better responds to H_2S gas at 250 ^{0}C, to at NH_3 150 ^{0}C, to Acetone 300 ^{0}C, to C_2H_5OH 300 ^{0}C, and to CO_2 350 ^{0}C, and to H_2 at 350 ^{0}C. The sensitivity towards each gas depends on temperature. The same sensor could be used to identify H_2S, NH_3, Acetone, Ethanol, CO_2 and H_2 just by varying the operating temperature. This is the most desirable characteristic of this sensor.

5.2.2. Active Region of the Sensor

The film was exposed to varying concentrations of H_2S. For the $ZnFe_2O_4$ samples, the response values were observed to increase continuously with increasing gas concentrations up to 1400 ppm, in Fig. 10. The rate of increase in response was relatively larger up to 1000 ppm and slowed down beyond 1000 ppm. Thus, the active region of the sensor would be up to 1000 ppm. At lower gas concentration, the unimolecular layer of gas molecules would be formed on the surface of the sensor, which could interact more actively giving larger response. The multilayer of gas molecules, on the sensors surface, at higher gas concentration would result in saturation in response beyond 1000 ppm gas.

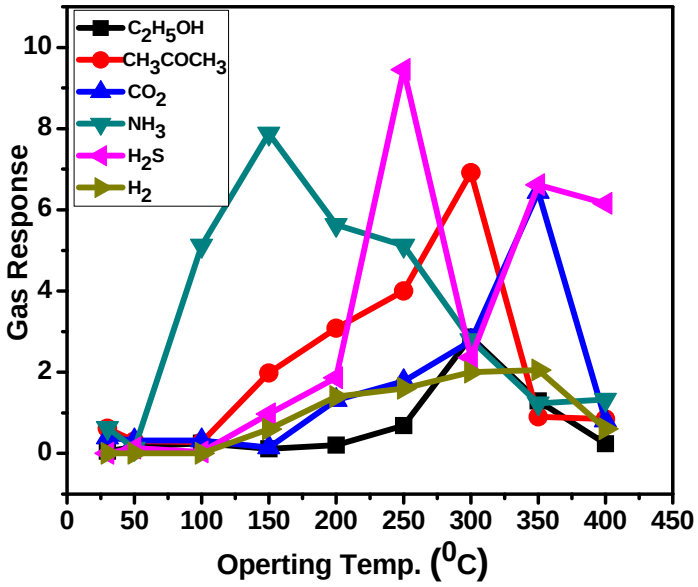

Fig. 9. Variation of gas response of $ZnFe_2O_4$with operating temperature.

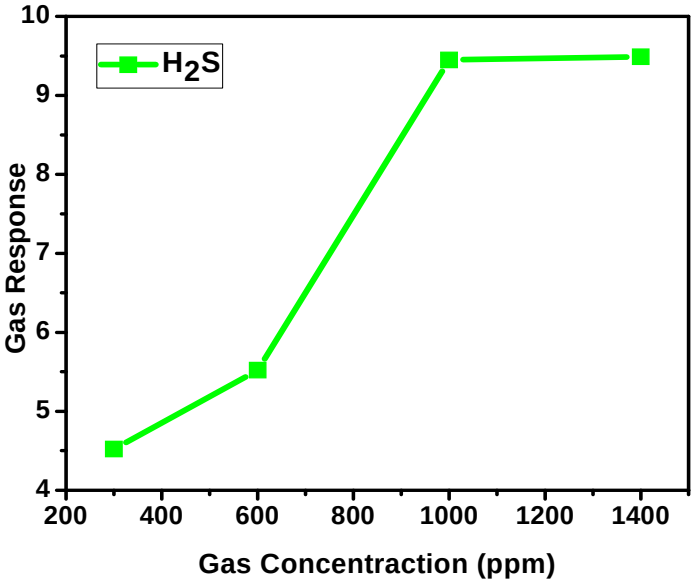

Fig. 10. Variation of gas response with gas concentration.

5.2.3. Selectivity

Fig. 11 depicts the, selectivity of the $ZnFe_2O_4$ film for 1000 ppm of various gases at various temperatures. That in contrast to $ZnFe_2O_4$, the sample showed not only enhanced response but also very high selectivity as shown in table below.

C_2H_5OH	CH_3COCH_3	CO_2	NH_3	H_2S	H_2
0.68	4.00	1.78	5.12	9.45	1.60

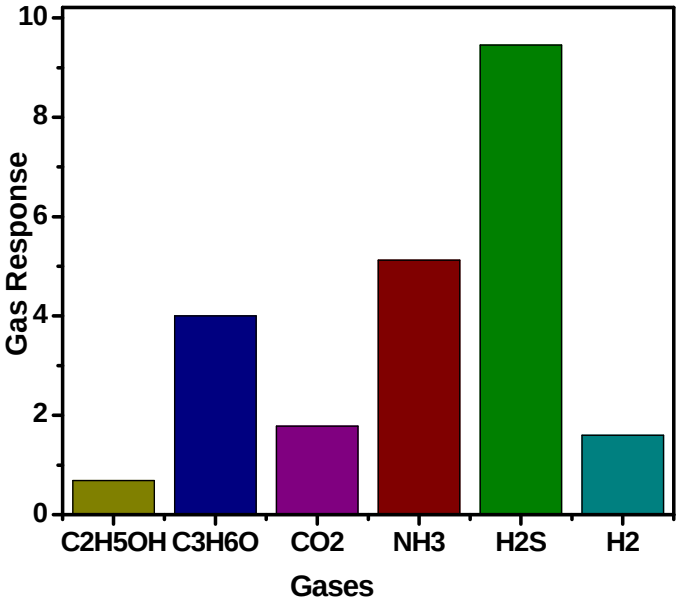

Fig. 11. Selectivity of $ZnFe_2O_4$ thick film among various gases.

5.2.4. Response and Recovery Time

The response of $ZnFe_2O_4$ sensor was found to be quick (~ 12 s) to 1000 ppm H_2S, while the recovery was fast (~ 30 s). The fast response may be due to faster oxidation of the gas. The negligible quantity of the surface reaction product and its high volatility explains its fast response and quick recovery to its initial chemical status.

6. Discussion

When reducing gases such as ammonia, ethanol, hydrogen, acetone, H_2S react with different oxygen species, complex series of reactions take place, ultimately oxidizing the ammonia, ethanol, hydrogen, acetone, and H_2S as:

$$C_2H_5OH + 6O^- + 300^0C \rightarrow 3H_2O + 2CO_2 + 6e^-$$
$$4NH_3 + 3O_2^- + 150^0C \rightarrow 6H_2O + 2N_2 + 3e^-$$
$$4H_2S + 4O^{2-} + 300^0C \rightarrow SO_2 + 4H_2O + 8e^-$$
$$2H^+ + 2O_2^- \rightarrow H_2O_2 + O_2$$

This shows n-type conduction mechanism. Thus on oxidation, a single molecule of gas liberates plurality of electrons in the conduction band, resulting in an increase in conductivity of the sensor. We found that the gas responses increase with operating temperature, reach to their responses increase with operating temperature, reach to their respective maxima at a particular temperature and then decrease with a further increase in operating temperature. An increase in operating temperature causes oxidation of a large number of gas molecules, producing a very large number of electrons. Therefore, the conductivity increases this is the reason why the gas response increases with operating temperature. The temperature at which the gas response is maximum is the actual temperature needed to activate the material for progressing the reaction. However, the response decreases at higher operating temperature, as the oxygen adsorbates are desorbed from the surface of the sensor. Also, at higher temperature, the carrier concentration increases due to intrinsic thermal excitation and the Debye length decreases. This may be one of the reasons for the decreased gas response at higher temperature [33].

The $ZnFe_2O_4$ film gives responses to H_2S gas at 250 ^{0}C, to at NH_3 150 ^{0}C, to acetone 300 ^{0}C, to C_2H_5OH 300 ^{0}C, to CO_2 350 ^{0}C, and to H_2 at 350 ^{0}C. The gas response can be tuned with operating temperature. The selective gas responses of the sensor to various gases at various temperatures may be attributed to oxidation of different gases by different oxygen species on the surface.

The working principal of thick film semiconducting gas sensors is based on the change of the electronic conductivity of the semiconducting material upon exposure of target gas. The interaction of target gas molecule with the surface of the thick film causes the transfer of electrons between the semiconducting surface and the adsorbates. The atmospheric oxygen molecules O_2 are adsorbed on the surface of the thick film. They capture the electrons from the conduction band of the thick film material as:

$$O_{2(air)} + 4e^- \rightarrow 2O^{2-}{}_{(film\ surface)}$$

The $ZnFe_2O_4$ showed response to hydrogen sulphide (H_2S) at high temperature. This would be attributed to the replacement of adsorbed oxygen by hydrogen sulphide (H_2S). Donating electrons to the base material reaction when hydrogen sulphide (H_2S) gas was exposed to $ZnFe_2O_4$ film, it substitutes lattice oxygen on the film surface. The reaction (7) is responsible for sensing of H_2S in which H_2S substituted for lattice oxygen to form $H_2S_{(ad)}^-$ inducing electron donation into the oxide.

$ZnFe_2O_4$ forms p–n heterojunctions, giving very high resistance even at room temperature. When $ZnFe_2O_4$ comes in contact with hydrogen sulphide gas, lattice oxygen would be replaced by hydrogen sulphide rupturing the heterojunctions and the resistance drops down suddenly. In addition to this, the material gain selections.

7. Summary

From the results, following statements can be made for the sensing performance of the present $ZnFe_2O_4$ sensors.

1. Nanocrystalline $ZnFe_2O_4$ has been synthesized by self combustion route. This synthesis route may be used for the synthesis of other metal oxide.
2. The phage formation of the ZnFe2O4 is investigated by TG-DTA, XRD, techniques. The synthesized product shows single phage of inverse spinel structure with an average diameter 15-35 nm.
3. Among all other additives ZnFe2O4 is outstanding in promoting the H2S gas.
4. ZnFe2O4 to be optimum and showed highest response to H2S gas at 250 ^{0}C.
5. The sensor showed very rapid response (~12 s) and recovery (~30 s) to H2S gas.
6. The sensor has good selectivity to H2S against NH3, acetone, CO2, H2, ethanol.

Acknowledgement

The author S. V. Bangale is thankful to IIT Bombay for providing the TEM facility during this research work.

References

[1]. N. S. Chen, X. J. Yang, E. S. Liu, J. L. Huang, Reducing gas-sensing properties of ferrite compounds MFe_2O_4 (M= Cu, Zn, Cd, and Mg), *Sens. Actuators B,* 66, 2000, pp. 178-180.

[2]. L. Pirlola, H. Parviainen, T. Hussein, A. Valli, K. Hameri, P. Aaalta, A. Virtanen, J. Keskinen, T. A. Pakkanen, T. Makela, R. E. Hillamo, *Atomos. Enviorn*., 38, 2004, pp. 3625-3635.
[3]. R. Nicolae, R. Elena, T. Florin, P. D. Popa, Some Spinel Oxide Compounds as Reducing Gas Sensors, *Sensors and Transducers*, Vol. 78, Issue 4, 2007, pp. 1134-1142.
[4]. X. Q. Liu, Z. L. Xu, Y. S. Shen, A new type ethanol material on $CdFe_2O_4$ semiconductor, *J. Yunnan Univ*., 19, 1997, pp. 147-149.
[5]. C. V. G. Reddy, S. V. Manorama and V. I. Rao, Semiconducting gas sensor for chlorine based on inverse spinel nickel ferrite, *Sensors and Actuators B*, 55, 1999, pp. 90-95.
[6]. D. R. Patil, L. A, Patil, Room temperature Chlorine gas sensing using surface modified ZnO thick film resistors, *Sensors and Actuators B,* 123, 2007, pp. 546-553.
[7]. D. R. Patil, L. A. Patil, P. P. Patil, Cr_2O_3-activated ZnO thick film resistors for ammonia gas sensing operable at room temperature, *Sens. Actuators B*, 126, 2007, pp. 368-374.
[8]. D. R. Patil, L. A. Patil, Al_2O_3- modified ZnO based thick film resistors for H_2 gas sensing, *Sensors & Transducers*, Vol. 81, 2007, pp. 1354-1363.
[9]. D. R. Patil, L. A. Patil, preparation and study of NH_3 gas sensing behavior of Fe_2O_3 doped ZnO thick film resistors, *Sensors & Transducers,* Vol. 70, 2006, pp. 661-670.
[10]. G. H. Jain, L. A. Patil, M. S. Wagh, S. A. Patil, D. R. Patil, D. P. Amalnerkar, Surface modified $BaTiO_3$ thick film resistors as H_2S gas sensor, *Sens. Actuators B*, 117, 2006, pp. 159-165.
[11]. N. S. Chen, X. J. Yang, E. S. Liu and J. L. Huang, reducing gas-sensing properties of ferrite compounds MFe_2O_4 (M = Cu, Zn, Cd, Mg), *Sensors and Actuators B,* 66, 2000, pp. 178-180.
[12]. C. V. Gopal, Reddy, S. V. Manorama, V. J. Rao, Preparation and characterization of ferrites as gas sensor materials, *J. Mater. Sci. Lett.*, 19, 2000, pp. 775-778.
[13]. Z. Jiao, M. H. Wu, J. Z. Gu, Z. Qin, Preparation and gas sensing characteristics of nanocrystalline spinel zinc ferrite thin films, *IEEE Sens. J.*, 3, 2003, pp. 435-438.
[14]. X. S. Niu, W. P. Du, W. M. Du, Preparation and gas sensing properties of ZnM_2O_4 (M = Fe, Co, Cr), *Sens. and Actuators B*, 99, 2004, pp. 405-409.
[15]. X. F. Chu, X. Q. Liu, G. Y. Meng, Effect of CdO dopant on the gas sensitivity properties of $ZnFe_2O_4$ semiconductors, *Sens. and Actuators B*, 65, 2000, pp. 64-67.
[16]. K. Arshak, I. Gaidan, Development of a novel gas sensor based on oxide thick film, *Mater. Sci. Eng. B*, 118, 2005, pp. 44-49.
[17]. G. Zhang, C. Li, F. Cheng, J. Chen, $ZnFe_2O_4$ tubes: Synthesis and application to gas sensors, *Sensors and Actuators B,* 120, 2007, pp. 403-410.
[18]. G. Y. Zhang, B. Guo, J. Chen, MCo_2O_4 (M = Ni, Cu, Zn), nanotubes, *Sens. and Actuators B,* 114, 2006, pp. 402-409.
[19]. N. B. Sonawane, D. R. Patil, L. A. Patil, CuO-Modified WO_3 sensors for the detection of a ppm level H_2S gas at room temperature, *Sensors & Transducers,* Vol. 93, 2008, pp. 42-91.
[20]. L. A. Patil, D. R. Patil, Heterocontact type CuO-modified SnO_2 sensor for the detection of a ppm level H_2S gas at room temperature, *Sens. Actuators B,* 120, 2006, pp. 316-323.
[21]. M. S. Wagh, L. A. Patil, Tanay Seth, D. P. Amalnerkar, Surface cupricated SnO_2-ZnO thick films as a H_2S gas sensor, *Mater. Chem. Phys.,* 84, 2004, pp. 228-233.
[22]. N. Yamazoe, S. Matsushima, T. Maekawa, J. Tamaki, N. Miura, Control of Pd-dispersion in SnO_2 based sensors, *Meas. Sci. Technol.,* 1, 1991, pp. 201-205.
[23]. V. Lantto, P. Romppainen, Response of some SnO_2 gas sensors to H_2S after quick cooling, *J. Electrochem. Soc.,* Vol. 135, No. 10, 1988, pp. 2550-2556.
[24]. W. Yuanda, T. Maosong, H. Xiuli, Z. Yushu, D. Guorui, Thin film sensors of SnO_2-CuO- SnO_2 sandwich structure to H_2S, *Sens. Actuators B,* 79, 2001, pp. 187-191.
[25]. J. Tamaki, Y. Yamada, Y. Yamamoto, M. Matsuoka, I. Ota, Sensing properties of dilute hydrogen sulphide of $ZnSb_2O_6$ thick film prepared by dip-coating method, *Sens. Actuators B,* 66, 2000, pp. 70-73.
[26]. S. V. Bangale, S. M. Khetre, S. R. Bamane**,** Synthesis, characterization and hydrophilic properties of nanocrystalline $ZnFe_2O_4$ oxide, *Archives of Applied Science Research,* 3, 2011, pp. 471-479.
[27]. S. V. Bangale, S. M. Khetre, S. R. Bamane, Synthesis, characterization and hydrophilic properties of nanocrystalline $ZnCo_2O_4$ oxide by combustion route, *Der Chemica Sinica,* 2, 2011, pp. 303-311.
[28]. M. S. Wagh, G. H. Jain, D. R. Patil, S. A. Patil and L. A. Patil, Modified zinc oxide thick film resistors as NH_3 gas sensors, *Sens. Actuators B,* 115, 2006, pp. 128-133.
[29]. L. A. Patil and D. R. Patil, Heterocontact type CuO-modified SnO_2 sensor for the detection of a ppm level H_2S gas at room temperature, *Sens. Actuators B,* 120, 2006, pp. 316-323.

[30]S. V. Bangale, S. R. Bamane, Nanostructured $ZnFe_2O_4$ Detection of Chlorine gas, *Sensors & Transducers*, Vol. 134, 2011, pp. 107-119.
[31].B. Cullity, Elements of X-ray diffraction, *Addison Weley*, London, 1956, pp. 99.
[32].C. Xiangfeng, L. Xinggin, Ethanol gas sensor based on $CoFe_2O_4$ nano-crystallines prepared by hydrothermal method, *Sensors and Actuators B*, 55, 1999, pp. 19-22.
[33].J. Mizsei, How can sensitive and selective semiconductor gas sensors be made, *Sens. Actuators B,* 23, 1995, pp. 173-176.
